Structure

Article

Monitoring the antibiotic darobactin modulating the β-barrel assembly factor BamA

Graphical Abstract

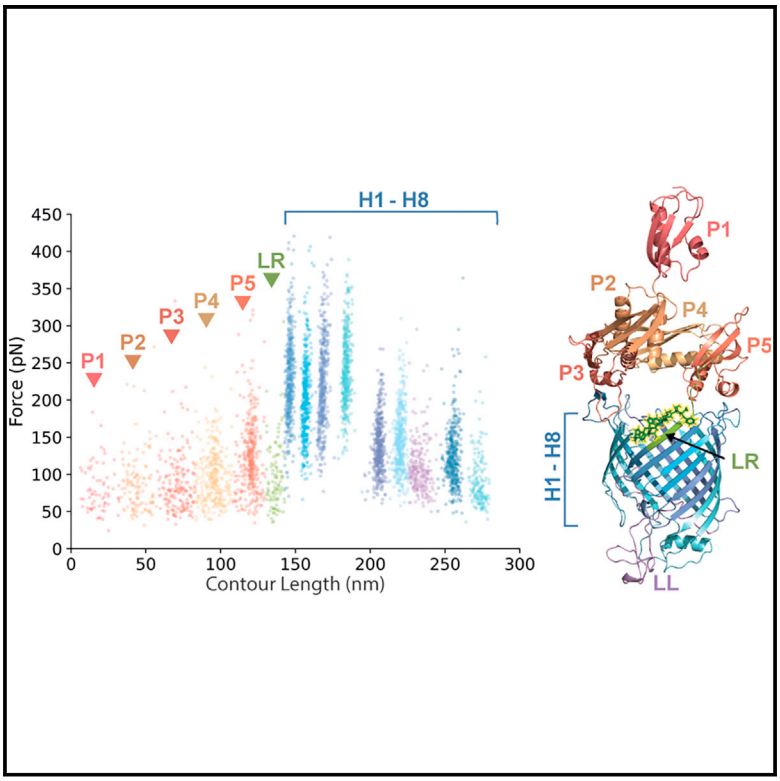

Authors

Noah Ritzmann, Selen Manioglu, Sebastian Hiller, Daniel J. Müller

Correspondence

daniel.mueller@bsse.ethz.ch

In brief

Ritzmann et al. employ SMFS to investigate BamA, the central unit of the BAM complex of *E. coli*. They quantify how the antibiotic darobactin modulates the mechanical, kinetic, and energetic properties of the POTRA domains, the linker domain, and the β-hairpins of the transmembrane β-barrel of BamA.

Highlights

- Mechanical, kinetic, and energetic properties of BamA
- Properties change upon binding to an antibiotic
- Structural regions change mechanical stability and lifetime
- Structural regions change free-energy and mechanical rigidity

Ritzmann et al., 2022, Structure *30*, 1–10
March 3, 2022
https://doi.org/10.1016/j.str.2021.11.004

CellPress

Structure

CellPress
OPEN ACCESS

Article

Monitoring the antibiotic darobactin modulating the β-barrel assembly factor BamA

Noah Ritzmann,[1] Selen Manioglu,[1] Sebastian Hiller,[2] and Daniel J. Müller[1,3,*]
[1]Department of Biosystems Science and Engineering, Eidgenössische Technische Hochschule (ETH) Zürich, Mattenstrasse 26, 4058 Basel, Switzerland
[2]Biozentrum, University of Basel, Spitalstrasse 41, 4056 Basel, Switzerland
[3]Lead contact
*Correspondence: daniel.mueller@bsse.ethz.ch
https://doi.org/10.1016/j.str.2021.11.004

SUMMARY

The β-barrel assembly machinery (BAM) complex is an essential component of *Escherichia coli* that inserts and folds outer membrane proteins (OMPs). The natural antibiotic compound darobactin inhibits BamA, the central unit of BAM. Here, we employ dynamic single-molecule force spectroscopy (SMFS) to better understand the structure-function relationship of BamA and its inhibition by darobactin. The five N-terminal polypeptide transport (POTRA) domains show low mechanical, kinetic, and energetic stabilities. In contrast, the structural region linking the POTRA domains to the transmembrane β-barrel exposes the highest mechanical stiffness and lowest kinetic stability within BamA, thus indicating a mechano-functional role. Within the β-barrel, the four N-terminal β-hairpins H1–H4 expose the highest mechanical stabilities and stiffnesses, while the four C-terminal β-hairpins H5–H6 show lower stabilities and higher flexibilities. This asymmetry within the β-barrel suggests that substrates funneling into the lateral gate formed by β-hairpins H1 and H8 can force the flexible C-terminal β-hairpins to change conformations.

INTRODUCTION

Integral outer membrane proteins (OMPs) of Gram-negative bacteria participate in a variety of crucial cellular functions, including nutrient transport (Klebba and Newton, 1998), protein secretion (Lauber et al., 2018), and adhesion (Heras et al., 2014). Most integral OMPs adopt a β-barrel conformation, which spans the outer membrane. In *Escherichia coli*, the insertion and folding of β-barrel proteins into the outer membrane is facilitated by the β-barrel assembly machinery (BAM) complex. The BAM complex consists of five protein components. These are BamA, an integral OMP and a member of the Omp85 superfamily (Gentle et al., 2004; Voulhoux et al., 2003), and four lipoproteins, BamB, BamC, BamD, and BamE, which are anchored to the inner leaflet of the outer membrane (Wu et al., 2005). BamA, the central component of the BAM complex, consists of a C-terminal 16-stranded transmembrane β-barrel domain and five periplasmic N-terminal polypeptide transport (POTRA) domains (Gentle et al., 2005; Sánchez-Pulido et al., 2003). Although all components of the BAM complex are necessary to efficiently insert proteins into the outer membrane (Hagan et al., 2010), only BamA and BamD are essential (Malinverni et al., 2006; Voulhoux et al., 2003).

The exact mechanism by which β-barrel OMPs are rapidly folded and integrated into the outer membrane by the BAM complex in the absence of an energy source such as ATP presumably occurs via the "budding model" but remains debated (Horne et al., 2020). The budding model proposes the formation of a hybrid β-barrel, formed by BamA and the OMP substrate, followed by the lateral release of the OMP into the membrane (Gruss et al., 2013; Noinaj et al., 2013). Recent structures of multiple folding intermediates support the budding model and extend the proposed process of BAM-mediated OMP folding and membrane insertion (Höhr et al., 2018; Lee et al., 2019; Tomasek et al., 2020). The first step of the insertion process is initiated by hydrogen bonding of a C-terminal signal sequence of the incoming substrate to the N-terminal β-strand of BamA (Lee et al., 2019; Robert et al., 2006; Xiao et al., 2021). β-sheets of the substrate are then thought to fold, starting from the C-terminus into the interior of the β-barrel. Upon reaching sufficient folding, the substrate is released into the outer membrane through a lateral gate formed by the first N-terminal and the last C-terminal β-strand of the transmembrane BamA β-barrel (Tomasek and Kahne, 2021). Compared to most other β-barrel-forming OMPs, the first and the last β-strand of the BamA β-barrel establish loose interactions. This results in a structurally dynamic region, referred to as the gate region, that takes a central role in inserting, folding, and releasing OMPs into the outer membrane (Noinaj et al., 2013). However, which mechanical and kinetic properties of the BamA β-barrel retain the unique dynamic state of the gate region remain to be characterized.

Because the BAM complex is essential for Gram-negative bacteria, it renders a promising antibiotic target. Compared to other essential components of Gram-negatives, the BAM complex is located at the cellular periphery and thus directly exposed to the external environment. Recently, the natural compound darobactin was identified to inhibit BamA. Darobactin is a bicyclic heptapeptide produced by *Photorhabdus*, found in the microbiome of

Please cite this article in press as: Ritzmann et al., Monitoring the antibiotic darobactin modulating the β-barrel assembly factor BamA, Structure (2021), https://doi.org/10.1016/j.str.2021.11.004

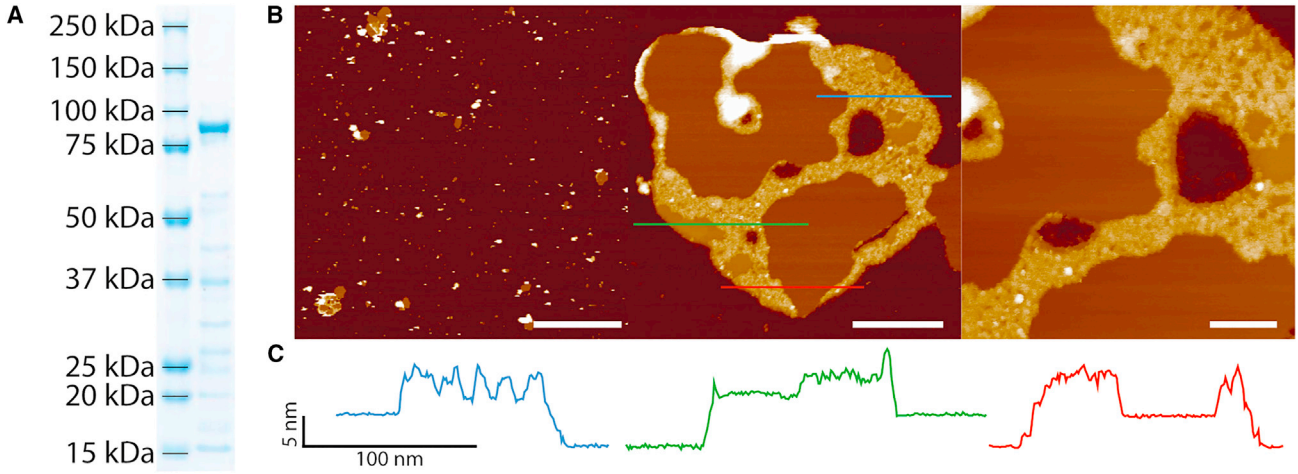

Figure 1. Biochemical analysis and AFM imaging of outer membrane vesicles (OMVs) enriched with BamA

(A) SDS gel of OMVs enriched with BamA, as characterized in this study (STAR Methods).

(B) AFM topographs of OMVs enriched with BamA. Upon adsorption to freshly cleaved mica, the OMVs open up and form planar membrane patches (left). Middle and right topographs, the densely packed areas of BamA appear higher (yellow, heights of ≈10–15 nm) than the surrounding membrane (heights of 5–8 nm). Blue, green, and red lines indicate height profiles taken for analysis (C). Scale bars from left to right represent 5 μm, 160 nm, and 130 nm, respectively. The full color range of the topographs corresponds to a vertical scale of 30 nm.

(C) Height profiles taken along the colored lines as indicated in the middle AFM topography.

entomopathogenic nematodes (Imai et al., 2019). The recent structure of the BAM complex bound to darobactin revealed darobactin binding to the functionally relevant gate region of the BamA β-barrel (Kaur et al., 2021). In order to inhibit BamA, darobactin mimics the C-terminal β-signal of native BamA substrates and binds to the first and last β-strand of the BamA β-barrel, which seals the lateral gate. Although the structure of the BamA-darobactin complex describes in great detail how darobactin inhibits BamA, it does not describe how darobactin affects the mechanical, kinetic, and energetic properties of BamA. Thus, quantifying how darobactin modulates these properties at a resolution of individual secondary structural elements would complement the structure of the BAM complex and allow us to draw a more complete picture of the darobactin-mediated BamA inhibition. Additionally, such insight is relevant for the targeted engineering of novel antibiotics, which could inhibit BamA similarly to darobactin.

Here, we characterize quantitatively and structurally how darobactin modulates the mechanical, kinetic, and energetic properties of BamA in the native outer membrane. Thereto, we apply atomic force microscopy (AFM)-based single-molecule force spectroscopy (SMFS), which allows us to quantify the mechanical properties of individual membrane proteins and to map them to their structural regions such as α-helices, β-hairpins, or polypeptide loops (Engel and Gaub, 2008; Oesterhelt et al., 2000; Thoma et al., 2017). The results provide an important and unique insight into the mechanisms by which darobactin inhibits BamA, guiding toward the mechanistic understanding of how to functionally inhibit BamA.

RESULTS

BamA stabilizes distinct structural segments

To characterize BamA in the native membrane, we prepared outer membrane vesicles (OMVs) enriched with BamA (Figure 1A). For SMFS, the OMVs were adsorbed to mica where they opened up and formed planar membrane patches with diameters ranging from 100 nm to 1 μm (Figure 1B). Membrane patches of densely packed BamA showed corrugated topographs, elevated 10–15 nm in height from the mica (Figure 1C). We then pushed the tip of the AFM cantilever onto BamA-enriched regions with a force of 1 nN for 0.5 s to promote the non-specific attachment of the tip to the N-terminal region (Thoma et al., 2018a, 2018bbib_Thoma_et_al_2018a) of BamA (Figure 2A). Upon the subsequent retraction of the cantilever from the membrane, we recorded force-distance (FD) curves. Occasionally, the FD curves recorded a sawtooth-like pattern of force peaks (Figure 2B), which was recently correlated to describe the stepwise unfolding of BamA (Thoma et al., 2018a, 2018b). Such FD curves showed the mechanical extension and stretching of the N-terminal region, which was followed by the stepwise unfolding of structural segments, until a single BamA was fully unfolded and extracted from the outer membrane. We repeated this procedure thousands of times to identify the reoccurring mechanical unfolding pattern specific to BamA in the absence of the antibiotic darobactin.

To compare the FD curves recorded upon mechanically unfolding single BamA, we aligned them in the force contour length space, where the prominent force peak at a contour length of 406 aa was used as a reference (Figures 2C and S1A). The alignment revealed 15 force peak classes (Figures 2D and S1B). Each of the force peak classes detected the unfolding of a structural segment of BamA in response to mechanical stress (Thoma et al., 2018a, 2018b). Counting from the N-terminal region, which was picked up by the AFM tip, we used the contour length of each force peak class to assign the structural segment BamA, unfolded in response to mechanical stress (Figure 2E). The first five force peak classes describe the unfolding of the five N-terminal POTRA domains of BamA (P1–P5), followed by the force peak class describing the short linker region (LR) between the

Please cite this article in press as: Ritzmann et al., Monitoring the antibiotic darobactin modulating the β-barrel assembly factor BamA, Structure (2021), https://doi.org/10.1016/j.str.2021.11.004

CellPress
OPEN ACCESS

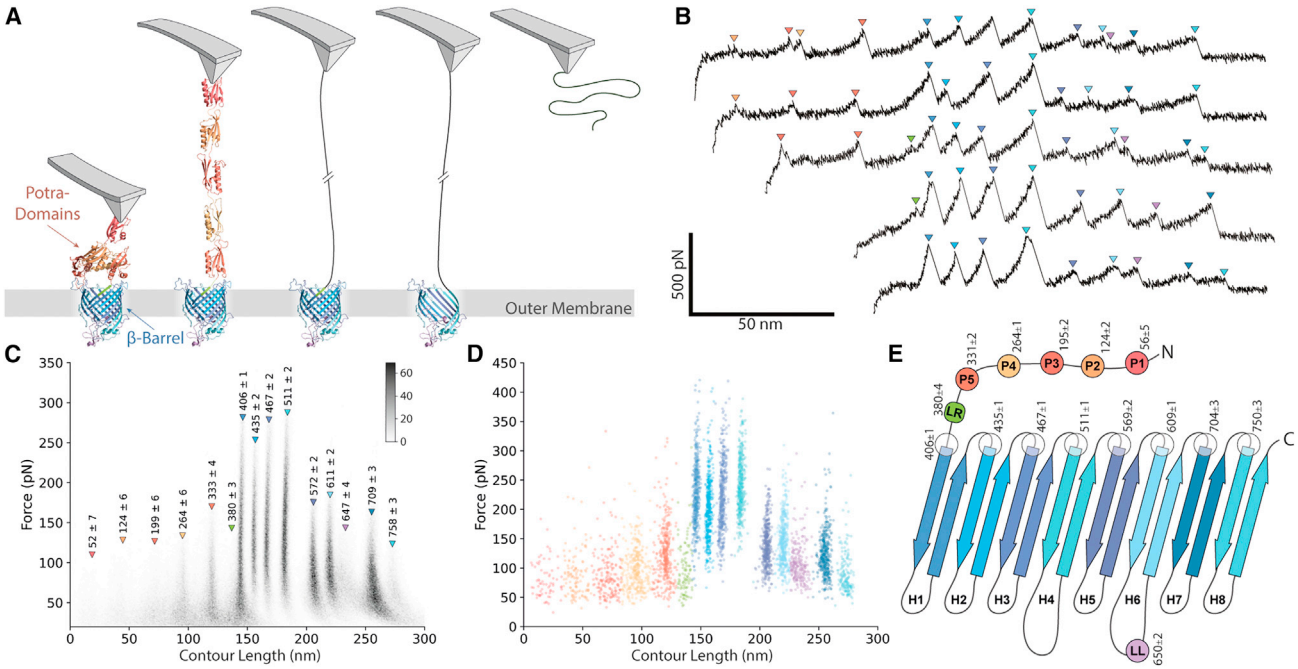

Figure 2. SMFS of BamA in native outer membrane

(A) Schematic representation of the mechanical unfolding of a single BamA from the native outer membrane by AFM-based SMFS. From left to right: the tip of the AFM cantilever is pushed onto the sample to establish unspecific interactions between the tip of the AFM cantilever and the N-terminal region of BamA. Retraction of the cantilever mechanically stretches the N-terminal region until it is fully extended. Further retraction of the cantilever results in the stepwise mechanical unfolding of individual structural segments of BamA, until it is completely extracted from the membrane.

(B) Exemplary FD curves recorded during the mechanical unfolding of single BamA by SMFS. Colored triangles indicate force peaks that denote unfolding events of BamA. This stepwise unfolding of structural segments continues until the entire BamA has been unfolded and extracted from the outer membrane.

(C) Density plot of 418 aligned and superimposed FD curves plotted in the force versus contour length space. The colored triangles indicate the force peak classes of BamA. Numbers above each triangle represent mean contour lengths and standard deviations of the respective force peak class in amino acids. The gray scale bar indicates the number of data points per bin.

(D) Force peak positions of all 418 FD curves shown in (C), plotted in the force versus contour length space. Each point indicates the force and contour length of a single rupture event, as indicated by the colored triangles in (B). Points with identical coloration belong to the same force peak class. The mean contour lengths and standard deviations are indicated in (C) for all force peak classes.

(E) Assignment of structural segment unfolded by BamA. Contour lengths of force peak classes (C, D) were located on the secondary structure (circles) and used to assign the structural segments of BamA. Mean contour lengths and standard deviations in amino acids are indicated next to each structural segment. The secondary structure of BamA is based on (PDB: 5D0O) (Gu et al., 2016).

See also Figures S1 and S2.

POTRA domain P5 and the transmembrane β-barrel. The next force peak classes are located in the β-barrel region of BamA and describe the unfolding of one β-hairpin after the other until the eight β-hairpins (H1–H8) are completely unfolded. One additional force peak class located between β-hairpins H6 and H7 corresponds to the unfolding of extracellular loop 6, which is locked in a lid-like (LL) structure to seal the β-barrel lumen from the extracellular space (Maier et al., 2015).

In summary, the FD curves recorded upon mechanically unfolding single BamA from the native outer membrane reveal a sequence of force peaks, each of which assigning the unfolding of a structural segment of the membrane protein. The forces at which each segment unfold are a direct measure of their mechanical stability.

Darobactin increases mechanical stability of BamA

Next, we unfolded BamA in the presence of darobactin in order to determine how darobactin binding changes the mechanical stability of BamA. At first sight, the force peak classes and thus the structural segments stabilizing BamA in the absence and presence of darobactin were very similar (Figures S1 and S2). Thus, darobactin did not change the structural segments BamA stabilizes against mechanical unfolding. Additionally, the mechanical forces required to unfold the individual POTRA domains were mostly unaffected by darobactin, except for POTRA domain P5, which increased from 136 pN to 149 pN (to ≈110%; Figure 3). Similarly, the mechanical stability of the LR increased weakly in the presence of darobactin. In large contrast, however, the forces required to mechanically unfold structural segments of the β-barrel region of BamA increased considerably in the presence of darobactin. In principle, every structural segment of the β-barrel, most of which representing a single β-hairpin, required higher forces to unfold than in the absence of darobactin. Upon adding up these forces, we found that 1.45 ± 0.15 nN (mean ± sd) was required to unfold all structural segments of the BamA β-barrel in the absence and that 1.67 ± 0.08 nN was required to completely unfold the β-barrel in the presence of darobactin.

Please cite this article in press as: Ritzmann et al., Monitoring the antibiotic darobactin modulating the β-barrel assembly factor BamA, Structure (2021), https://doi.org/10.1016/j.str.2021.11.004

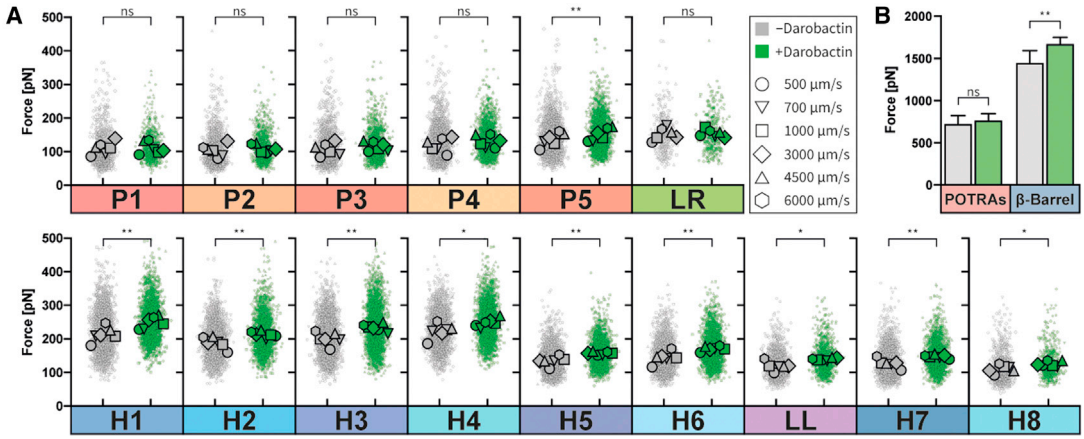

Figure 3. Unfolding forces of BamA in the absence and the presence of darobactin

(A) Forces required to mechanically unfold BamA in the absence (gray) and in the presence (green) of darobactin. The structural segments unfolded by BamA in response to mechanical force correspond to the POTRA domains P1–P5, the LR, the β-hairpins H1–H8 of the transmembrane β-barrel, and the LL structure in the extracellular loop 6. The datapoints within each plot show the forces of all unfolding force peaks belonging to the force peak class (Figure 2). The mean unfolding forces at different unfolding speeds are indicated by different markers. Statistical significances were calculated using two-tailed paired t-tests, comparing each pair of mean forces originating from the same pulling speed. $^{**}P < 0.01$; $^{*}P < 0.05$; ns, non-significant, $P \geq 0.05$.

(B) Mechanical stability of the POTRA domains and the β-barrel domain of BamA in the absence (gray) and presence (green) of darobactin. Bars represent the sum of the mean unfolding forces of all POTRA domains, including the gate class G, and of the β-barrel domain. Error bars indicate the standard deviation of the mean. Statistical significances were calculated using two-tailed paired t-tests comparing the summed up forces in the absence and in the presence of darobactin. $^{**}P < 0.01$; $^{*}P < 0.05$; ns, non-significant, $P \geq 0.05$.

Close inspection of the unfolding forces showed that the first four N-terminal β-hairpins H1–H4 were the most stable structural segments of the β-barrel, which further increased stability upon darobactin binding. Among the four N-terminal β-hairpins, the first β-hairpin H1 showed the highest mechanical stability, both in the absence and in the presence of darobactin. That H1 increases stability upon darobactin binding can be explained by the structural model, showing darobactin to bind to the gate region of BamA, located between the first β-strand and the last β-strand of the β-barrel domain (Kaur et al., 2021). However, the SMFS data also show that darobactin affected the mechanical stability of all other β-hairpins shaping the transmembrane β-barrel. Upon darobactin binding, the mechanical stability of the β-barrel domain increased to ≈116%, while the remaining structural segments increased stability to ≈106%. Similar effects have been observed in previous SMFS studies, where localized interactions established by the binding of a ligand or a molecular compound to a membrane protein could stabilize or destabilize structural regions not directly involved in the binding (Serdiuk et al., 2014; Spoerri et al., 2019).

In summary, the forces required to mechanically unfold structural segments of BamA increase upon darobactin binding. Thus, BamA increases mechanical stability, with the biggest increase observed for the first four N-terminal β-hairpins of the β-barrel domain. However, the observations also indicate that the localized binding of darobactin to BamA modulates the stability of structural regions distant from the binding site.

Darobactin modulates free-energy landscape

The mechanical forces at which proteins unfold depend on the pulling speed (i.e., the loading rate describing the force applied over time) (Bippes and Muller, 2011; Evans, 2001; Evans and Ritchie, 1997). In response to mechanically applied force membrane proteins, stepwise unfold structural segments (Bippes and Muller, 2011), such as that observed here for BamA. The mechanical properties and the kinetic or energetic stability of the structural segments at equilibrium (i.e., no force applied) can be approached by measuring their unfolding forces over a broad range of pulling speeds. We hence applied SMFS in the dynamic force spectroscopy (DFS) mode and mechanically unfolded BamA over a range of retraction speeds (Method Details) in the absence and presence of darobactin (Figures S1 and S2).

The DFS data show that the mean forces required to unfold individual structural segments of BamA increase linearly with the logarithm of the loading rate (Figures 4 and S3). Fitting the Bell-Evans model (Bell, 1978; Evans, 2001; Evans and Ritchie, 1997) to the DFS plots allows us to extrapolate the mechanical, kinetic, and energetic properties of each structural segment at equilibrium (Bippes and Muller, 2011). The fits approximate that the distance x_u that every structural segment has to be stretched along the pulling trajectory to reach the transition state toward unfolding and the unfolding rate k_0. The x_u values can be used to describe the width of the free-energy valley hosting the folded state of a structural segment (Serdiuk et al., 2014). Accordingly, a larger x_u value describes a wider free-energy valley that can host a larger number of conformational substates of the structural segment. The reciprocal of k_0 represents the lifetime of a structural segment. Using x_u and k_0, the height of the free-energy barrier $\Delta G_u^{\ddagger}$ stabilizing a structural segment against unfolding and the mechanical stiffness κ (i.e., spring constant) of the segment can be calculated. These free-energy landscape parameters, which were approximated for each structural segment of BamA in the presence and in the absence of darobactin (Table 1), are described in the following.

Please cite this article in press as: Ritzmann et al., Monitoring the antibiotic darobactin modulating the β-barrel assembly factor BamA, Structure (2021), https://doi.org/10.1016/j.str.2021.11.004

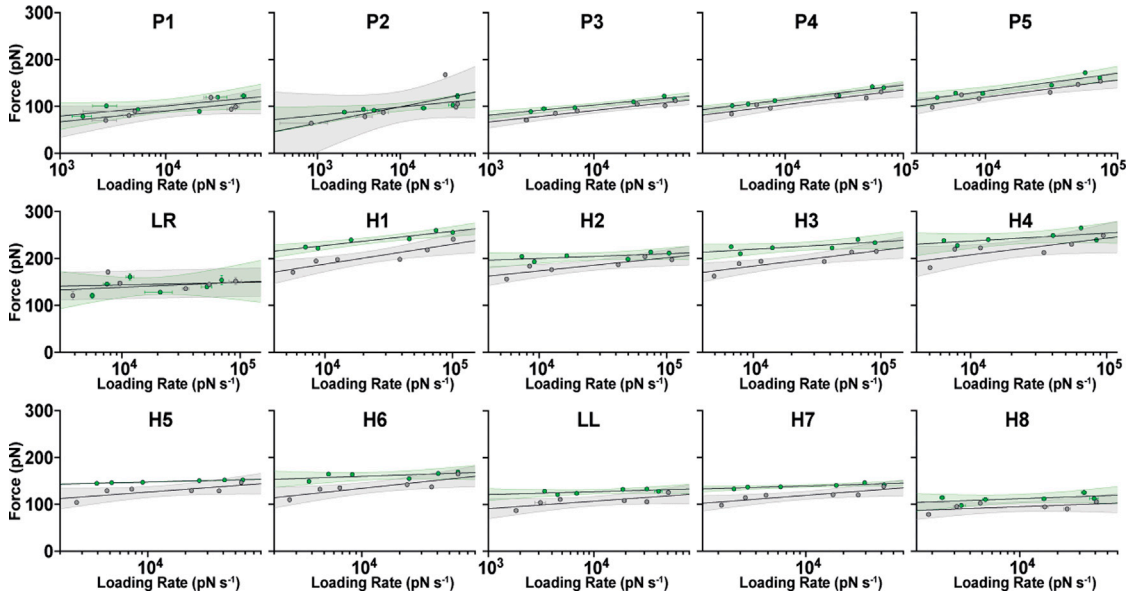

Figure 4. Estimating the free-energy landscape parameters of the structural segments of BamA in the absence and the presence of darobactin by DFS

The DFS plots show the mean unfolding forces versus the mean loading rates (data points) of each structural segment in the absence (gray) and the presence (green) of darobactin. Black lines result from fitting the Bell-Evans model (Bell, 1978; Evans, 2001; Evans and Ritchie, 1997) to the data with the shaded areas, indicating the 95% confidence bands. Error bars represent the standard error of each data point. Free-energy parameters x_u and k_0 obtained from the fits are given in Table 1. Raw data underlying the DFS plots are shown in Figure S3. See also Figure S3.

Darobactin widens free-energy wells

The x_u values of the five POTRA domains increased from 0.32 nm to 0.39 nm (to ≈122%) in the presence of darobactin (Table 1). The only POTRA domain, which slightly decreased x_u upon darobactin binding was P5. Among all structural segments of BamA, the LR showed the smallest x_u values in the absence (0.17 nm) and presence (0.20 nm) of darobactin. In contrast, the structural segments (e.g., β-hairpins) of the transmembrane β-barrel region widened their free-energy wells from 0.33 nm to 0.76 nm (to ≈235%) in the presence of darobactin. The strongest increase in x_u was observed for β-hairpin H6, which moved its distance to the transition state from the initial 0.33 nm to 1.05 nm and thus increased the width of the free-energy well to 315%.

The results show that darobactin binding to BamA only slightly widens the x_u values of the POTRA domains and the LR, but considerably increases the x_u values of the β-barrel domain. Thus, darobactin binding increases the x_u value of almost every structural segment of BamA. Consequently, the free-energy valleys accommodating the structural segments widen so that they could host more and/or different conformational states. Amongst all structural segments of BamA, the region linking the POTRA domains to the transmembrane β-barrel show the smallest x_u values, thus indicating to display the smallest conformational variability amongst all segments in the absence and in the presence of darobactin.

Darobactin increases kinetic stability

On average, the POTRA domains decreased their k_0 values to 24% in the presence of darobactin and thus considerably increased their lifetimes (Table 1). Amongst all structural segments of BamA, the LR showed the largest k_0 value of 1.05 s^{-1} in the absence of darobactin, which upon darobactin binding, reduced to 0.53 s^{-1}. In stark contrast, the structural segments (e.g., β-hairpins) of the β-barrel of BamA decreased on average their k_0 values to 6% in the presence of darobactin.

In summary, every structural segment of BamA lowers the unfolding rate k_0 and thus increases lifetime upon darobactin binding. Naturally, by their insertion into the outer membrane, the β-hairpins of the transmembrane β-barrel expose high lifetimes, which in the presence of darobactin, is further increased by orders of magnitude. In contrast, the shortest lifetime is observed for the polypeptide stretch linking the POTRA domains to the transmembrane β-barrel.

Darobactin increases energetic stability

Darobactin binding of BamA increased the free-energy barriers stabilizing the structural segments against mechanical unfolding (Table 1). On average, the β-hairpins of the BamA β-barrel increased their $\Delta G_u^{\ddagger}$ values drastically from 25.8 k_BT in the absence to 45.0 k_BT in the presence of darobactin. Whereas the weakest free-energy barrier increase in individual β-hairpins was to 103% (H8), the strongest increase was to 229% (H5), and the average increase in all β-hairpins forming the β-barrel was to 171%. At the same time, the average $\Delta G_u^{\ddagger}$ values of the POTRA domains and the LR increased slightly from 21.7 k_BT to 23.7 k_BT.

Taken together, whereas the free-energy barriers of all β-hairpins and the LL structure of the β-barrel increase on average to 171% upon darobactin binding, the POTRA domains and the gate region increase the free-energy barriers on average to only 109%. We thus conclude that the binding of darobactin to BamA considerably increases the energetic stability of the β-barrel but only slightly that of the soluble POTRA domains and LR.

Please cite this article in press as: Ritzmann et al., Monitoring the antibiotic darobactin modulating the β-barrel assembly factor BamA, Structure (2021), https://doi.org/10.1016/j.str.2021.11.004

Table 1. Free-energy landscape parameters of the structural segments of BamA in the absence and in the presence of darobactin

		x_u (nm)		k_0 (s^{-1})		$\Delta G_u^{\ddagger}$ (k_BT)		κ (Nm^{-1})	
Segment	CL (aa)	–Darobactin	+Darobactin	–Darobactin	+Darobactin	–Darobactin	+Darobactin	–Darobactin	+Darobactin
P1	56 ± 5	0.41 ± 0.18	0.44 ± 0.18	0.13 ± 0.45	0.02 ± 0.10	22.80 ± 3.58	24.47 ± 4.10	1.12 ± 0.98	1.06 ± 0.90
P2	124 ± 2	0.27 ± 0.14	0.54 ± 0.18	0.94 ± 2.85	0.00 ± 0.01	20.79 ± 3.03	26.45 ± 4.02	2.30 ± 2.41	0.75 ± 0.51
P3	195 ± 2	0.38 ± 0.06	0.44 ± 0.05	0.18 ± 0.22	0.02 ± 0.02	22.42 ± 1.19	24.75 ± 1.28	1.24 ± 0.38	1.05 ± 0.27
P4	264 ± 1	0.29 ± 0.06	0.30 ± 0.03	0.46 ± 0.68	0.15 ± 0.12	21.49 ± 1.46	22.61 ± 0.76	2.11 ± 0.91	2.00 ± 0.39
P5	331 ± 2	0.26 ± 0.05	0.25 ± 0.04	0.33 ± 0.43	0.19 ± 0.24	21.84 ± 1.32	22.37 ± 1.25	2.67 ± 0.99	2.95 ± 0.97
LR	380 ± 4	0.17 ± 0.03	0.20 ± 0.07	1.05 ± 1.04	0.53 ± 1.21	20.68 ± 0.99	21.36 ± 2.30	5.69 ± 1.95	4.40 ± 3.11
H1	406 ± 0	0.22 ± 0.05	0.31 ± 0.05	0.02 ± 0.05	$2.3 \times 10^{-5} \pm 6.7 \times 10^{-5}$	24.60 ± 2.34	31.43 ± 2.96	4.09 ± 1.94	2.64 ± 0.94
H2	435 ± 1	0.34 ± 0.10	0.96 ± 0.60	$5.1 \times 10^{-4} \pm 2.1 \times 10^{-3}$	$1.4 \times 10^{-17} \pm 4.1 \times 10^{-16}$	28.30 ± 4.03	59.54 ± 29.30	2.03 ± 1.19	0.53 ± 0.72
H3	467 ± 1	0.28 ± 0.07	0.59 ± 0.26	$2.4 \times 10^{-3} \pm 7.5 \times 10^{-3}$	$3.4 \times 10^{-11} \pm 4.7 \times 10^{-10}$	26.74 ± 3.07	44.84 ± 13.82	2.78 ± 1.42	1.07 ± 1.00
H4	511 ± 1	0.27 ± 0.10	0.55 ± 0.32	$9.1 \times 10^{-4} \pm 4.6 \times 10^{-3}$	$1.8 \times 10^{-11} \pm 3.3 \times 10^{-10}$	27.73 ± 5.09	45.48 ± 18.57	3.20 ± 2.53	1.22 ± 1.50
H5	569 ± 2	0.48 ± 0.21	1.46 ± 0.00	$4.7 \times 10^{-4} \pm 2.9 \times 10^{-3}$	$5.7 \times 10^{-20} \pm 3.7 \times 10^{-21}$	28.38 ± 6.04	65.04 ± 0.06	1.02 ± 0.90	0.25 ± 0.00
H6	609 ± 1	0.33 ± 0.10	1.05 ± 0.75	0.02 ± 0.05	$5.6 \times 10^{-15} \pm 1.6 \times 10^{-13}$	24.88 ± 3.00	53.55 ± 28.55	1.85 ± 1.12	0.40 ± 0.61
LL	650 ± 2	0.32 ± 0.14	0.47 ± 0.28	0.05 ± 0.20	$3.5 \times 10^{-4} \pm 2.9 \times 10^{-3}$	23.75 ± 4.04	28.69 ± 8.34	1.90 ± 1.73	1.07 ± 1.29
H7	704 ± 3	0.45 ± 0.14	1.23 ± 0.36	$2.2 \times 10^{-3} \pm 8.1 \times 10^{-3}$	$2.4 \times 10^{-15} \pm 2.9 \times 10^{-14}$	26.83 ± 3.64	54.38 ± 11.74	1.08 ± 0.67	0.29 ± 0.18
H8	750 ± 3	0.23 ± 0.09	0.26 ± 0.15	0.53 ± 1.31	0.30 ± 1.20	21.35 ± 2.45	21.93 ± 4.03	3.18 ± 2.50	2.68 ± 3.17

For each structural segment of BamA, the force peak positions are indicated by the contour lengths (CL) in amino acids (aa). The parameters x_u, k_0, $\Delta G_u^{\ddagger}$, and κ are obtained from the DFS plots, which were recorded in the absence (–) and the presence (+) of darobactin (Figure 4). All values give mean ± sd.

Darobactin decreases stiffness

In the absence of darobactin, the spring constants κ of the five POTRA domains ranged from 1.12 N m^{-1} (P1) to 2.67 N m^{-1} (P5) (Table 1). Among all POTRA domains, P1–P4 considerably decreased stiffness (to ≈77%) upon darobactin binding. One exception was POTRA domain P5, which slightly increased stiffness from 2.67 to 2.95 N m^{-1} (to ≈111%). Among all structural segments of BamA, the LR showed the highest stiffness both in the unbound (5.69 N m^{-1}) and in the darobactin-bound (4.40 N m^{-1}) state. In the absence of darobactin, the structural segments representing individual β-hairpins of the transmembrane β-barrel showed spring constants ranging from 1.02 N m^{-1} (H5) to 4.09 N m^{-1} (H1). Upon darobactin binding, the β-hairpins considerably decreased spring constants now ranging from 0.25 N m^{-1} (H5) to 2.68 N m^{-1} (H8). The largest relative decrease in mechanical stiffness was measured for β-hairpin H6, which lowered from 1.85 N m^{-1} (unbound state) to 0.40 N m^{-1} (to ≈22%). In the presence of darobactin, structural segments of the β-barrel on average reduced their spring constants to ≈42% of their initial values.

In summary, upon darobactin binding, BamA reduces the structural stiffness of almost every structural segment. In the unbound state, the mechanically stiffest segments are the LR and the N-terminal β-hairpin H1. Additionally, the C-terminal β-hairpin H8, which together with H1, forms the gate region of BamA, shows a relatively high spring constant (mechanical stiffness) in the unbound state. Upon darobactin binding, we find that these and the other β-hairpins of the transmembrane β-barrel region considerably reduce mechanical stiffness.

DISCUSSION

SMFS experiments on integral β-barrel OMPs have thus far observed common mechanical unfolding pathways. By applying a mechanical pulling force to one terminal end, individual β-hairpins forming the transmembrane β-barrel unfold and extract sequentially from the membrane. This sequential unfolding of β-hairpins was observed for several OMPs, including OmpA (Bosshart et al., 2012b), OmpG (Sapra et al., 2009), FhuA (Thoma et al., 2012), LamB (Thoma et al., 2017), and BamA (Thoma et al., 2018a, 2018b). The findings presented here confirm the previous studies. The extensive data recorded in our study allow us to identify an additional force peak class of BamA, which locates between the POTRA domains and the β-barrel and is referred to as LR. Thus, upon mechanically pulling its N-terminal end, BamA displays 15 distinct force peak classes, each originating from the mechanical unfolding of a structural segment. The soluble POTRA domains and the LR, which are located at the N-terminus of BamA, unfold first at comparably low forces. Afterwards, the region linking POTRA domains and transmembrane β-barrel unfolds. Eight of the nine following force peak classes correspond to the mechanical unfolding of individual β-hairpins and display relatively high mechanical stability, such as that previously measured for other OMPs (Thoma et al., 2012, 2017).

Please cite this article in press as: Ritzmann et al., Monitoring the antibiotic darobactin modulating the β-barrel assembly factor BamA, Structure (2021), https://doi.org/10.1016/j.str.2021.11.004

CellPress
OPEN ACCESS

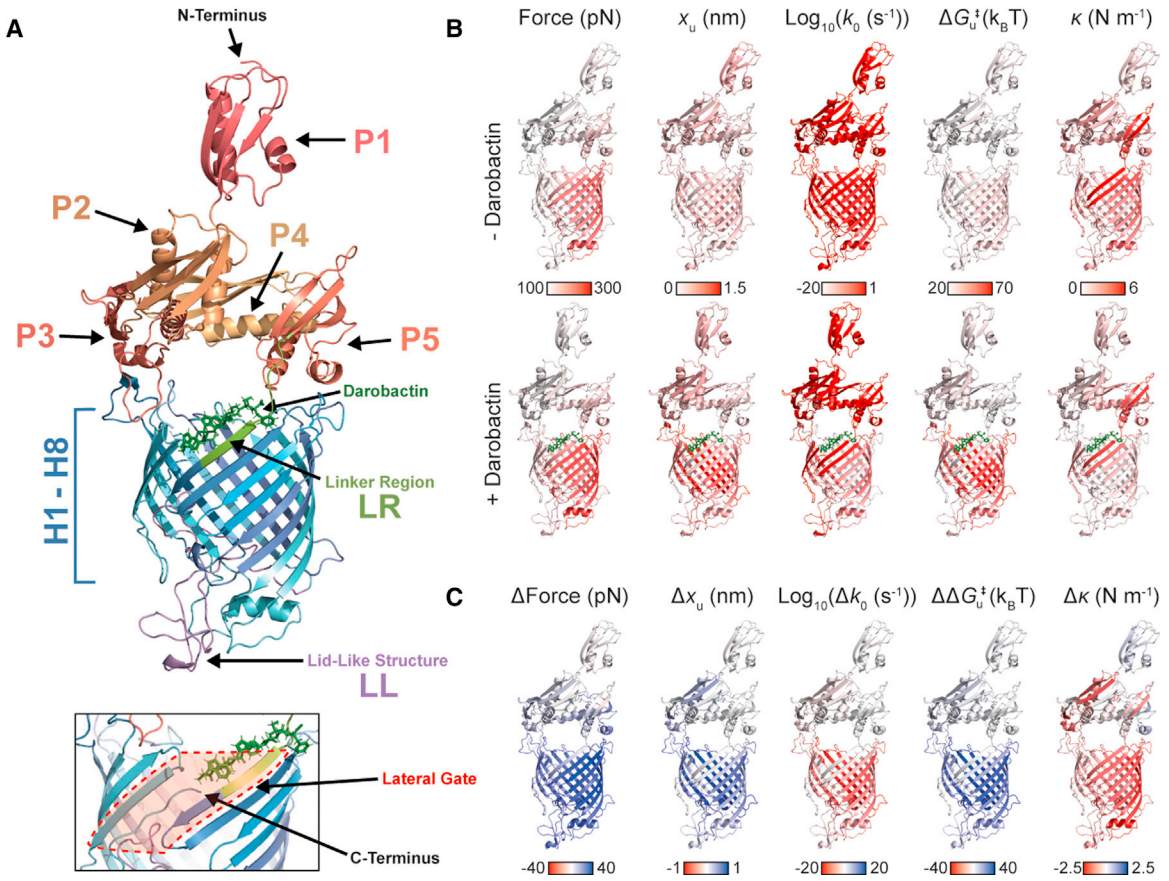

Figure 5. Effect of darobactin on the mechanical and energetic properties of BamA

(A) Structure of BamA bound to darobactin (PDB: 7NRI) (Kaur et al., 2021). Darobactin is shown in green. Colored segments of BamA represent force peak classes, which were assigned to structural segments, as shown in Figure 2. Both termini are indicated in black. Inset at the bottom shows the lateral gate of BamA, indicated by the red area.

(B) Mapping the forces required to mechanically unfold BamA and the parameters describing the free-energy landscape to the unliganded (PDB: 5D0O) (Gu et al., 2016) and to the darobactin-bound BamA structure.

(C) Mapping the relative changes in the forces required to mechanically unfold BamA and in the parameters describing the free-energy landscape induced by darobactin to the BamA structure.

Upon mechanically unfolding BamA in the absence and in the presence of darobactin, we observe the same 15 force peak classes, describing the same sequential unfolding pathways (Figure S4). This observation indicates that a characteristic network of interactions stabilizes the same structural segments of BamA in the absence and presence of darobactin. The finding is in full agreement with the structural model of BamA that shows no large structural rearrangement upon darobactin binding (Kaur et al., 2021). However, the force peak classes recorded in the presence of darobactin display increased unfolding forces (to ≈116%) as compared to those recorded in the absence of darobactin. Thus, darobactin considerably increases the mechanical stability of BamA. This stabilizing effect is most prominent for the β-barrel region of BamA (Figure 5). Thereby, the first four N-terminal β-hairpins H1–H4 were the most stable β-hairpins with the first N-terminal β-hairpin H1 showing the highest mechanical stability. This observation indicates that the first β-hairpin H1 forms a mechanically stable gate together with the last C-terminal β-hairpin H8 of the BamA β-barrel. Upon binding to this gate region, darobactin further stabilizes β-hairpins H1 and H8 as well as the other β-hairpins of the β-barrel. However, darobactin also increases the stability of the only essential POTRA domain P5 (Bos et al., 2007). Although the structural model does not provide conclusive evidences for a specific interaction of POTRA domain P5 and darobactin, our data show that the properties of POTRA domain P5 are modulated via the darobactin-mediated inhibition of BamA. Interestingly, it has been previously observed that darobactin-resistant strains show mutations of residue F394 in the POTRA domain P5 (Imai et al., 2019). The darobactin-dependent modulation of the mechanical stability of P5 thus adds insight into the manifold interactions of darobactin with BamA.

To further investigate the complex effects of darobactin on the structural properties of BamA, we employed SMFS in the dynamic mode. For every structural segment of BamA, we find a linear relationship between the mean unfolding force and the logarithm of the mean loading rate. This suggests that the folded state of every segment is separated from the unfolded state by a single free-energy barrier (Evans and Ritchie, 1997). We observe the general trend that darobactin increases the distance

to the transition state (x_u values), increases the lifetime, enhances the free-energy barrier, but lowers the mechanical stiffness (or rigidity) of almost every structural segment of BamA (Figure 5). As these changes apply at different magnitudes in the structural segments, we will discuss them as follows in detail.

One prominent effect is observed for the structural region linking the POTRA domains to the transmembrane β-barrel. This LR shows the lowest kinetic stability amongst all structural segments of BamA in the absence and presence of darobactin. Interestingly, the LR also shows the smallest transition state distances in the absence and presence of darobactin, thus indicating to adopt the smallest conformational variability amongst all structural segments of BamA. Moreover, the LR exposes the highest spring constant amongst all structural segments of BamA, thus showing the highest mechanical stiffness. Together, the low kinetic stability and conformational variability and the high mechanical stiffness of the LR provide important functional insight into how the POTRA domains connect to the β-barrel domain.

Another remarkable insight is provided for the transmembrane β-barrel. Although darobactin increases the height of every free-energy barrier stabilizing a structural segment of BamA (Figure 5), which means that all segments stabilize energetically, the highest increase (to ≈171%) was observed for the structural segments (e.g., β-hairpins) of the transmembrane β-barrel. In the unbound state, the mechanically stiffest segments of BamA are the LR and the N-terminal β-hairpin H1. Additionally, the N-terminal β-hairpins H2, H3, and H4 and the C-terminal β-hairpin H8 show a relatively high mechanical stiffness in the unbound state. Comparatively, β-hairpins H5–H7 are among the mechanically most flexible regions of BamA. This suggests that if a substrate is funneled into the membrane by the two relatively stiff and stable β-hairpins H1 and H8, which form the lateral gate of BamA, the β-hairpins H5–H7 provide a mechanically flexible region such as that needed to enlarge the transmembrane β-barrel and to insert and fold the substrate. As darobactin considerably changes the mechanical stiffnesses of almost every structural region of BamA as well as their mechanical, kinetic, and energetic stabilities, these fine-tuned properties come out of balance. Particularly, the stiffnesses of all structural segments of the β-barrel decrease. In summary, the data thus show that in the presence of darobactin, the β-barrel domain of BamA increases its relatively high energetic stability and decreases its mechanical stiffness to structurally soften. Most importantly, however, darobactin binds between β-hairpins H1 and H8, thus sealing the lateral gate to prevent substrate inclusion (Kaur et al., 2021).

Taken together, we observe darobactin to mechanically stabilize BamA considerably. The stabilizing effects are most prominent for the entire β-barrel domain of BamA, although darobactin only binds to the lateral gate region (Kaur et al., 2021). The free-energy landscape parameters characterizing the properties of every structural segment of BamA describe how darobactin modulates the mechanical, kinetic, and energetic properties of BamA in great detail (Figure 5). Together with the structural models of BamA in the unbound state and in the darobactin-bound state, the parameters provide mechanistic insight into how the rather complex BamA machinery is inhibited. Further SMFS studies may be conducted in the presence of β-signals of varying OMPs to investigate how transient interactions modulate the mechanical, kinetic, and energetic properties of BamA in contrast to darobactin. Similarly, the effects of different antibiotic compounds targeting the BAM complex could be studied by SMFS to elaborate on current findings. Gaining a deeper understanding of different factors shaping BamA-mediated OMP insertion and folding will be beneficial for the rational design of novel antibiotic compounds against the BAM complex and will hopefully advance our efforts to resolve the current antimicrobial resistance crisis.

Further information and requests for resources and reagents should be directed to and will be fulfilled by the lead contact, Daniel J. Müller (daniel.mueller@bsse.ethz.ch).

STAR★METHODS

Detailed methods are provided in the online version of this paper and include the following:

- KEY RESOURCES TABLE
- RESOURCE AVAILABILITY
  - Lead contact
  - Materials availability
  - Data and code availability
- EXPERIMENTAL MODEL AND SUBJECT DETAILS
- METHOD DETAILS
  - Cloning
  - Preparation of outer membrane vesicles (OMVs) enriched with BamA
  - Single-molecule force spectroscopy (SMFS) and dynamic force spectroscopy (DFS)
  - Force–distance curve-based AFM (FD-Based AFM) imaging of OMVs
- QUANTIFICATION AND STATISTICAL ANALYSIS
  - SMFS data analysis

SUPPLEMENTAL INFORMATION

Supplemental information can be found online at https://doi.org/10.1016/j.str.2021.11.004.

ACKNOWLEDGMENTS

This work was supported by the Swiss National Science Foundation, the NCCR Molecular Systems Engineering, and the Swiss Nanoscience Institute (SNI).

AUTHOR CONTRIBUTIONS

N.R. performed cloning, prepared outer membrane vesicles, conducted SMFS experiments, and analyzed all data. S.M. recorded high-resolution AFM images. N.R., S.H., and D.J.M. designed the study and discussed and wrote the manuscript.

DECLARATION OF INTERESTS

The authors declare no competing interests.

Received: September 10, 2021
Revised: October 30, 2021
Accepted: November 11, 2021
Published: December 6, 2021

REFERENCES

Alsteens, D., Pfreundschuh, M., Zhang, C., Spoerri, P.M., Coughlin, S.R., Kobilka, B.K., and Müller, D.J. (2015). Imaging G protein-coupled receptors

while quantifying their ligand-binding free-energy landscape. Nat. Methods *12*, 845–851.

Ankerst, M., Breunig, M.M., Kriegel, H.P., and Sander, J. (1999). OPTICS: ordering points to identify the clustering structure. ACM SIGMOD Rec. *28*, 49–60.

Bell, G.I. (1978). Models for the specific adhesion of cells to cells. Science *200*, 618–627.

Bippes, C.A., and Muller, D.J. (2011). High-resolution atomic force microscopy and spectroscopy of native membrane proteins. Rep. Prog. Phys. *74*, 1–43.

Bos, M.P., Robert, V., and Tommassen, J. (2007). Functioning of outer membrane protein assembly factor Omp85 requires a single POTRA domain. EMBO Rep. *8*, 1149–1154.

Bosshart, P.D., Frederix, P.L.T.M., and Engel, A. (2012a). Reference-free alignment and sorting of single-molecule force spectroscopy data. Biophys. J. *102*, 2202–2211.

Bosshart, P.D., Iordanov, I., Garzon-Coral, C., Demange, P., Engel, A., Milon, A., and Müller, D.J. (2012b). The transmembrane protein KpOmpA anchoring the outer membrane of Klebsiella pneumoniae unfolds and refolds in response to tensile load. Structure *20*, 121–127.

Bustamante, C., Marko, J.F., Siggia, E.D., and Smith, S. (1994). Entropic elasticity of lambda-phage DNA. Science *265*, 1599–1600.

Butt, H.J., and Jaschke, M. (1995). Calculation of thermal noise in atomic force microscopy. Nanotechnology *6*, 1–7.

Cormack, B., and Castaño, I. (2002). Introduction of point mutations into cloned genes. Methods Enzymol. *350*, 199–218.

Engel, A., and Gaub, H.E. (2008). Structure and mechanics of membrane proteins. Annu. Rev. Biochem. *77*, 127–148.

Evans, E. (2001). Probing the relation between force - lifetime - and chemistry in single molecular bonds. Annu. Rev. Biophys. Biomol. Struct. *30*, 105–128.

Evans, E., and Ritchie, K. (1997). Dynamic strength of molecular adhesion bonds. Biophys. J. *72*, 1541–1555.

Gentle, I., Gabriel, K., Beech, P., Waller, R., and Lithgow, T. (2004). The Omp85 family of proteins is essential for outer membrane biogenesis in mitochondria and bacteria. J. Cell Biol. *164*, 19–24.

Gentle, I.E., Burri, L., and Lithgow, T. (2005). Molecular architecture and function of the Omp85 family of proteins. Mol. Microbiol. *58*, 1216–1225.

Gruss, F., Zähringer, F., Jakob, R.P., Burmann, B.M., Hiller, S., and Maier, T. (2013). The structural basis of autotransporter translocation by TamA. Nat. Struct. Mol. Biol. *20*, 1318–1320.

Gräter, F., Shen, J., Jiang, H., Gautel, M., and Grubmüller, H. (2005). Mechanically induced titin kinase activation studied by force-probe molecular dynamics simulations. Biophys. J. *88*, 790–804.

Gu, Y., Li, H., Dong, H., Zeng, Y., Zhang, Z., Paterson, N.G., Stansfeld, P.J., Wang, Z., Zhang, Y., Wang, W., et al. (2016). Structural basis of outer membrane protein insertion by the BAM complex. Nature *531*, 64–69.

Hagan, C.L., Kim, S., and Kahne, D. (2010). Reconstitution of outer membrane protein assembly from purified components. Science *328*, 890–892.

Heras, B., Totsika, M., Peters, K.M., Paxman, J.J., Gee, C.L., Jarrott, R.J., Perugini, M.A., Whitten, A.E., and Schembri, M.A. (2014). The antigen 43 structure reveals a molecular Velcro-like mechanism of autotransporter-mediated bacterial clumping. Proc. Natl. Acad. Sci. U. S. A. *111*, 457–462.

Horne, J.E., Brockwell, D.J., and Radford, S.E. (2020). Role of the lipid bilayer in outer membrane protein folding in Gram-negative bacteria. J. Biol. Chem. *295*, 10340–10367.

Höhr, A.I.C., Lindau, C., Wirth, C., Qiu, J., Stroud, D.A., Kutik, S., Guiard, B., Hunte, C., Becker, T., Pfanner, N., et al. (2018). Membrane protein insertion through a mitochondrial β-barrel gate. Science *359*, 1–12.

Imai, Y., Meyer, K.J., Iinishi, A., Favre-Godal, Q., Green, R., Manuse, S., Caboni, M., Mori, M., Niles, S., Ghiglieri, M., et al. (2019). A new antibiotic selectively kills Gram-negative pathogens. Nature *576*, 459–464.

Kaur, H., Jakob, R.P., Marzinek, J.K., Green, R., Imai, Y., Bolla, J.R., Agustoni, E., Robinson, C.V., Bond, P.J., Lewis, K., et al. (2021). The antibiotic darobactin mimics a β-strand to inhibit outer membrane insertase. Nature *593*, 125–129.

Klebba, P.E., and Newton, S.M.C. (1998). Mechanisms of solute transport through outer membrane porins: burning down the house. Curr. Opin. Microbiol. *1*, 238–248.

Lauber, F., Deme, J.C., Lea, S.M., and Berks, B.C. (2018). Type 9 secretion system structures reveal a new protein transport mechanism. Nature *564*, 77–82.

Lebigot, E.O. (2018). Uncertainties: a Python package for calculations with uncertainties. http://pythonhosted.org/uncertainties/.

Lee, J., Tomasek, D., Santos, T.M., May, M.D., Meuskens, I., and Kahne, D. (2019). Formation of a β-barrel membrane protein is catalyzed by the interior surface of the assembly machine protein BamA. eLife *8*, e49787.

Maier, T., Clantin, B., Gruss, F., Dewitte, F., Delattre, A.S., Jacob-Dubuisson, F., Hiller, S., and Villeret, V. (2015). Conserved Omp85 lid-lock structure and substrate recognition in FhaC. Nat. Commun. *6*, 1–9.

Malinverni, J.C., Werner, J., Kim, S., Sklar, J.G., Kahne, D., Misra, R., and Silhavy, T.J. (2006). YfiO stabilizes the YaeT complex and is essential for outer membrane protein assembly in Escherichia coli. Mol. Microbiol. *61*, 151–164.

MuellerLabETHZ. (2021). MuellerLabETHZ/BamA_darobactin: Content of BamA_Darobactin (v1.0.0) (Zenodo). https://doi.org/10.5281/zenodo.5647099.

Noinaj, N., Kuszak, A.J., Gumbart, J.C., Lukacik, P., Chang, H., Easley, N.C., Lithgow, T., and Buchanan, S.K. (2013). Structural insight into the biogenesis of β-barrel membrane proteins. Nature *501*, 385–390.

Oesterhelt, F., Oesterhelt, D., Pfeiffer, M., Engel, A., Gaub, H.E., and Müller, D.J. (2000). Unfolding pathways of individual bacteriorhodopsins. Science *288*, 143–146.

Pedregosa, F., Varoquaux, G., Gramfort, A., Michel, V., Thirion, B., Grisel, O., Blondel, M., Prettenhofer, P., Weiss, R., Dubourg, V., et al. (2011). Scikit-learn: machine learning in Python. J. Mach. Learn. Res. *12*, 2825–2830.

Pfreundschuh, M., Martinez-Martin, D., Mulvihill, E., Wegmann, S., and Muller, D.J. (2014). Multiparametric high-resolution imaging of native proteins by force-distance curve-based AFM. Nat. Protoc. *9*, 1113–1130.

Prilipov, A., Phale, P.S., Van Gelder, P., Rosenbusch, J.P., and Koebnik, R. (1998). Coupling site-directed mutagenesis with high-level expression: large scale production of mutant porins from E. coli. FEMS Microbiol. Lett. *163*, 65–72.

Robert, V., Volokhina, E.B., Senf, F., Bos, M.P., Van Gelder, P., and Tommassen, J. (2006). Assembly factor Omp85 recognizes its outer membrane protein substrates by a species-specific C-terminal motif. Plos Biol. *4*, 1984–1995.

Sapra, K.T., Damaghi, M., Köster, S., Yildiz, Ö., Kühlbrandt, W., and Müller, D.J. (2009). One β hairpin after the other: exploring mechanical unfolding pathways of the transmembrane β-barrel protein OmpG. Angew. Chem. *121*, 8456–8458.

Serdiuk, T., Madej, M.G., Sugihara, J., Kawamura, S., Mari, S.A., Kaback, H.R., and Müller, D.J. (2014). Substrate-induced changes in the structural properties of LacY. Proc. Natl. Acad. Sci. U. S. A. *111*, 1571–1580.

Spoerri, P.M., Sapra, K.T., Zhang, C., Mari, S.A., Kato, H.E., Kobilka, B.K., and Müller, D.J. (2019). Conformational plasticity of human protease-activated receptor 1 upon antagonist- and agonist-binding. Structure *27*, 1517–1526.

Sánchez-Pulido, L., Devos, D., Genevrois, S., Vicente, M., and Valencia, A. (2003). POTRA: a conserved domain in the FtsQ family and a class of β-barrel outer membrane proteins. Trends Biochem. Sci. *28*, 523–526.

Thoma, J., Bosshart, P., Pfreundschuh, M., and Müller, D.J. (2012). Out but not in: the large transmembrane β-barrel protein FhuA unfolds but cannot refold via β-hairpins. Structure *20*, 2185–2190.

Thoma, J., Ritzmann, N., Wolf, D., Mulvihill, E., Hiller, S., and Müller, D.J. (2017). Maltoporin LamB unfolds β hairpins along mechanical stress-dependent unfolding pathways. Structure *25*, 1139–1144.

Thoma, J., Manioglu, S., Kalbermatter, D., Bosshart, P.D., Fotiadis, D., and Müller, D.J. (2018a). Protein-enriched outer membrane vesicles as a native platform for outer membrane protein studies. Commun. Biol. *1*, 1–9.

Thoma, J., Sun, Y., Ritzmann, N., and Müller, D.J. (2018b). POTRA domains, extracellular lid, and membrane composition modulate the

conformational stability of the β barrel assembly factor BamA. Structure *26*, 987–996.

Tomasek, D., and Kahne, D. (2021). The assembly of β-barrel outer membrane proteins. Curr. Opin. Microbiol. *60*, 16–23.

Tomasek, D., Rawson, S., Lee, J., Wzorek, J.S., Harrison, S.C., Li, Z., and Kahne, D. (2020). Structure of a nascent membrane protein as it folds on the BAM complex. Nature *583*, 473–478.

Voulhoux, R., Bos, M.P., Geurtsen, J., Mols, M., and Tommassen, J. (2003). Role of a highly conserved bacterial protein in outer membrane protein assembly. Science *299*, 262–265.

Wu, T., Malinverni, J., Ruiz, N., Kim, S., Silhavy, T.J., and Kahne, D. (2005). Identification of a multicomponent complex required for outer membrane biogenesis in Escherichia coli. Cell *121*, 235–245.

Xiao, L., Han, L., Li, B., Zhang, M., Zhou, H., Luo, Q., Zhang, X., and Huang, Y. (2021). Structures of the β-barrel assembly machine recognizing outer membrane protein substrates. FASEB J. *35*, 1–13.

Zocher, M., Fung, J.J., Kobilka, B.K., and Müller, D.J. (2012). Ligand-specific interactions modulate kinetic, energetic, and mechanical properties of the human β2 adrenergic receptor. Structure *20*, 1391–1402.

Please cite this article in press as: Ritzmann et al., Monitoring the antibiotic darobactin modulating the β-barrel assembly factor BamA, Structure (2021), https://doi.org/10.1016/j.str.2021.11.004

STAR★METHODS

KEY RESOURCES TABLE

REAGENT or RESOURCE	SOURCE	IDENTIFIER
Bacterial and virus strains		
BL21(DE3)omp8	(Prilipov et al., 1998)	N/A
Chemicals, peptides, and recombinant proteins		
LB Agar, powder (Lennox L agar)	Thermo Fisher Scientific	Cat# 22700025
Ampicillin sodium salt	Sigma-Aldrich	Cat# A9518
LB medium (Difco)	Becton Dickinson	Cat# BD 244610
Isopropyl-β-D-thiogalactoside	Sigma-Aldrich	Cat# I6758
Dulbecco's phosphate buffered saline with added magnesium and calcium	Sigma-Aldrich	Cat# D8662
Deposited data		
Structure of BamA complex	(Gu et al., 2016)	PDB: 5D0O
Structure of BamA bound to darobactin	(Kaur et al., 2021)	PDB: 7NRI
Oligonucleotides		
Step1_fwd: 5'-GCGTGGCGGCTCTGGTTCCGGT TCTGCTGAAGGGTTCGTAGTGA-3'	This Work	N/A
Step1_rev: 5'-CCAGAGCCGCCACG CGCAGAAAA GAAACCGTATACGGTGGCGC-3'	This Work	N/A
Step2_fwd: 5'-GGTAACGAAGAAGGCTTCTTTTCT GCGCGTGG-3'	This Work	N/A
Step2_rev: 5'-GAAGCCTTCTTCGTTACCGTATAC GGTGGCG-3'	This Work	N/A
Recombinant DNA		
pY161	(Thoma et al., 2018a, 2018b)	N/A
Software and algorithms		
Pymol (Version 2.4.2)	Schrodinger	http://www.pymol.org
Prism (Version 8.4.3)	Graphpad Software	http://www.graphpad.com
SMFS Data Analysis Procedure	(Thoma et al., 2017) and this work	N/A
Nanoscope Analysis software (version 1.8)	Bruker	http://nanoscaleworld.bruker-axs.com/nanoscaleworld/
Other		
OMCL-RC800PSA cantilevers	Olympus	Cat# OMCL-RC800PSA
450 nm filter unit	Merck Millipore	Cat# S2HVU02RE
Python codes for FD curve analysis of the data published in this work	This Work	https://doi.org/10.5281/zenodo.5647099

RESOURCE AVAILABILITY

Lead contact

Further information and requests for resources and reagents should be directed to and will be fulfilled by the lead contact, Daniel J. Müller (daniel.mueller@bsse.ethz.ch)

Materials availability

This study did not generate new unique reagents. Plasmids and bacterial strains produced in this study will be available upon request.

Data and code availability

All data reported in this paper will be shared by the lead contact upon request.

Please cite this article in press as: Ritzmann et al., Monitoring the antibiotic darobactin modulating the β-barrel assembly factor BamA, Structure (2021), https://doi.org/10.1016/j.str.2021.11.004

All original code has been deposited at Zenodo and is publicly available as of the date of publication (MuellerLabETHZ, 2021). DOIs are listed in the key resources table.

Any additional information required to reanalyze the data reported in this paper is available from the lead contact upon request.

EXPERIMENTAL MODEL AND SUBJECT DETAILS

E. coli BL21(DE3)omp8 (Prilipov et al., 1998) were used to prepare outer membrane vesicles under culture conditions as described in Method Details.

METHOD DETAILS

Cloning

Plasmid pNR48, which was used to overexpress BamA into the *E. coli* outer membrane was cloned in two steps, in which an N-terminal flexible linker was attached to facilitate unfolding experiments. First the sequence coding for FFSARGGSGSGS was inserted into plasmid pY161 (Thoma et al., 2018a, 2018b) after the N-terminal periplasmic export sequence using primers.

5'-GCGTGGCGGCTCTGGTTCCGGTTCTGCTGAAGGGTTCGTAGTGA-3' and.

5'-CCAGAGCCGCCACGCGCAGAAAAGAAACCGTATACGGTGGCGC-3' with the QuikChange PCR method (Cormack and Castaño, 2002). In a second step the sequence coding for NEEG was inserted in front of the newly inserted sequence with primers 5'-GGTAACGAAGAAGGCTTCTTTTCTGCGCGTGG-3' and.

5'-GAAGCCTTCTTCGTTACCGTATACGGTGGCG-3' again using the QuikChange PCR method.

Preparation of outer membrane vesicles (OMVs) enriched with BamA

The plasmid pNR48 was transformed into *E. coli* BL21(DE3)omp8 (Prilipov et al., 1998). OMVs were prepared as described[54]. Briefly, the *E. coli* were grown on a Luria-Bertani (LB) Agar plate (Lennox L Agar, Invitrogen) supplemented with 100 μg ml^{-1} ampicillin (Ampicillin sodium salt, Sigma) at 37°C. A single colony was picked and grown over night in LB medium (Difco, Becton Dickinson) supplemented with 100 μg ml^{-1} ampicillin at 37°C under constant shaking at 220 rpm. 300 ml LB medium in a baffled Erlenmeyer flask containing 100 μg ml^{-1} ampicillin were inoculated 1:100 with the overnight culture and grown at 37°C, 220 rpm while the optical density at 600 nm (OD_{600}) was closely monitored. Overexpression of BamA was induced with 1 mM isopropyl-β-D-thiogalactopyranoside (IPTG, Sigma) when $OD_{600} \approx 0.4$ was reached. After induction the cells were incubated until the onset of saturation in growth was reached. The cells were removed by centrifugation at 10'000 xg for 10 min. The supernatant was sterile-filtered using a 450 nm filter unit (Merk Millipore) and stored overnight at 4°C. On the following day, OMVs were collected by centrifugation at 38'400 xg for 1.5 h and resuspended in 12 ml Dulbecco's phosphate buffered saline with added magnesium and calcium (DPBSS, Sigma). The OMVs were washed in an additional centrifugation step at 108'000 xg for 1 h and resuspended in 1 ml of DPBSS. The resulting solution was stored in aliquots at –80°C.

Single-molecule force spectroscopy (SMFS) and dynamic force spectroscopy (DFS)

For each SMFS experiment, an aliquot containing 5 μl OMVs in DPBSS was thawed at 4°C and filled up to 50 μl with DPBSS. The sample was centrifuged for 15 min at 16'100 xg at 4°C and the pellet was resuspended in 40 μl DPBSS. 5 μl of the resulting sample were diluted in 45 μl DPBSS and adsorbed to freshly cleaved mica. After 15 min the sample was rinsed several times with DPBSS to remove non-adsorbed material. The sample was filled up to 1.5 ml and covered with a silicon skirt to prevent evaporation. SMFS was performed at ≈25°C using a commercial AFM (Nanowizard II Ultra, JPK Instruments) and OMCL-RC800PSA cantilevers (Olympus), which were calibrated with the thermal noise method (Butt and Jaschke, 1995). Membrane patches were located by contact mode AFM imaging. The tip of the AFM cantilever was pushed onto densely packed regions of the membrane for 500 ms with a force of 1 nN to non-specifically attach BamA. DFS was conducted at six different retraction speeds (500, 700, 1'000, 3'000, 4'500 and 6'000 nm s^{-1}). At least five different cantilevers were used for each experimental condition to minimize errors due to uncertainties in cantilever spring constant calibration. SMFS experiments conducted at different retraction speeds were recorded in mixed and random order to reduce the influence of external factors on the experimental outcome. For SFMS in presence of darobactin, the sample preparation, AFM imaging and SMFS were conducted in DPBSS containing 20 μM darobactin. An external 16-bit data acquisition card (NI PCI-6221, National Instruments) was used to record SMFS data at high-frequencies.

Force–distance curve-based AFM (FD-Based AFM) imaging of OMVs

OMVs enriched with BamA were diluted (1:50) in DPBSS and adsorbed onto freshly cleaved mica for 15 min at room temperature. After the adsorption, the sample was gently washed with DPBSS to remove non-adsorbed membranes. FD-based AFM imaging of OMVs was performed with a Nanoscope Multimode 8 (Bruker, USA) operated in PeakForce Tapping mode in DPBSS at room temperature as described (Pfreundschuh et al., 2014; Thoma et al., 2018a, 2018b). In FD-based AFM, the AFM cantilever approaches and retracts from a biological sample while raster-scanning in a pixel-by-pixel manner to record FD curves. Thereby the distance of the cantilever tip and the sample distance is measured for each pixel to estimate the height profile of the sample topography. The AFM was placed in a temperature-controlled acoustic isolation box and equipped with a 120-μm piezoelectric J scanner and fluid cell. AFM topographs were recorded using PEAKFORCE-HiRs-F-A (Bruker Nano Inc., USA) cantilevers having a nominal spring

constant of 0.4 N m^{-1}, a resonance frequency of ≈165 kHz in liquid, and a sharpened silicon tip with a nominal radius of ≈1 nm. Before imaging, cantilevers were calibrated by ramping on the mica surface and the thermal noise method (Butt and Jaschke, 1995). AFM topographs were recorded by applying an imaging force of 100–120 pN at 2 kHz oscillation frequency, with a vertical oscillation amplitude of 30 nm and a resolution of 512×512 pixels. Image post-processing and analysis were performed using the Nanoscope Analysis software v.1.8.

QUANTIFICATION AND STATISTICAL ANALYSIS

SMFS data analysis

For each experimental condition, the FD curves were transformed to force *versus* contour length space using the worm-like chain (WLC) model (Bustamante et al., 1994),

$$F(x) = \frac{k_B T}{P} = \left[\frac{1}{4}\left(1 - \frac{x}{L}\right)^{-2} - \frac{1}{4} + \frac{x}{L}\right] \quad \text{(Equation 1)}$$

where k_B is the Boltzmann constant, T the absolute temperature in Kelvin, P the average polypeptide persistence length (assuming a length of 0.36 nm per amino acid (aa)), x the extension in nm and L the polypeptide contour length in aa. A fixed persistence length of 0.4 nm was used (Bosshart et al., 2012a). The BamA unfolding curves were aligned to each other in force versus contour length space using a self-written software. In the next step the position of every force peak in every FD curve was detected. To assign individual force peaks to force peak classes, we used the OPTICS clustering from scikit learn (Ankerst et al., 1999; Pedregosa et al., 2011) to automatically cluster the force peaks of one SMFS data set recorded at 1'000 nm s^{-1} retraction speed in presence of darobactin. After the force peak positions were clustered and the mean contour lengths determined, we used the resulting force peak clusters as a template to classify the FD curves recorded under other experimental conditions.

The aligned and classified FD curves were analyzed as described (Spoerri et al., 2019; Thoma et al., 2017). Briefly, the loading rate of every force peak was determined by the slope of a linear fit to the last data points before of the rupture event described by the respective force peak in the force-time curve (Alsteens et al., 2015). For each experimental condition the rupture forces and loading rates of all force peaks belonging to a force peak class were binned and the resulting histograms were fitted with Gaussians to determine the most probable rupture force and loading rate (Figure S3). The resulting means and standard errors of each force peak class were fitted with the Bell-Evans model (Bell, 1978; Evans, 2001; Evans and Ritchie, 1997),

$$F^* = \frac{k_B T}{x_u} ln\left(\frac{x_u r}{k_B T k_0}\right) \quad \text{(Equation 2)}$$

where F^* is the most probable rupture force in pN and r is the loading rate in pN s^{-1} (Figure 4). Both values allowed to approximate the distance x_u, separating the free-energy valley of the folded structural segment from the unfolded state, and the unfolding rate k_0 of the structural segment. The parameter $\Delta G_u^{\ddagger}$ describing the height of the free-energy barrier stabilizing a structural segment against unfolding was calculated using

$$\Delta G_u^{\ddagger} = -k_B T ln(\tau_A k_0) \quad \text{(Equation 3)}$$

where τ_A is the Arrhenius frequency (Gräter et al., 2005), for which we chose 10^{-8} s^{-1} (Zocher et al., 2012). The parameter κ, which describes the stiffness of a structural segment, was calculated by:

$$\kappa = \frac{2\Delta G_u^{\ddagger}}{x_u^2} \quad \text{(Equation 4)}$$

Errors were propagated using the python uncertainties package (Lebigot, 2018).